Available online at www.sciencedirect.com
SCIENCE DIRECT®
Journal of Sound and Vibration 262 (2003) 752–768
JOURNAL OF SOUND AND VIBRATION
www.elsevier.com/locate/jsvi

Letter to the Editor

A deformable body dynamic analysis of planetary gears with thin rims

A. Kahraman*, A.A. Kharazi, M. Umrani

Center for Gear Research, Department of Mechanical, Industrial and Manufacturing Engineering, The University of Toledo, Mail Stop 312, Nitschke Hall 4045, Toledo, OH 43606-3390, USA

Received 11 March 2002; accepted 26 October 2002

1. Introduction

Planetary gear sets are used commonly by automotive and aerospace industries. Typical applications include jet propulsion systems, rotorcraft transmissions, passenger vehicle automatic transmissions and transfer cases and off-highway vehicle gearboxes. Their high-power-density design combined with their kinematic flexibility in achieving different speed ratios make planetary gears sets often preferable to counter-shaft gear reduction systems.

As planetary gear sets possess unique kinematic and geometric properties, they require specialized design knowledge [1]. One type of the key parameters, the rim thickness of the gears, must be defined carefully by the designer in order to meet certain design objectives regarding power density, planet load sharing, noise and durability. From the power density point of view, the rim of the each gear forming the planetary gear set must be as thin as possible in order to minimize mass. Besides reducing mass, added gear flexibility through reduced rim thickness was shown to reduce the influence of a number of internal gear and carrier errors, and piloting inaccuracies [2]. In addition, it was also reported that a flexible internal gear helps improve the load sharing amongst the planets when a number of manufacturing and assembly related gear and carrier errors are present [3–6]. Many of these effects of flexible gear rims were quantified under quasi-static conditions in the absence of any dynamic effects.

The effect of rim thickness on gear stresses attracted significant attention in the past. A number of theoretical studies [7–14] modelled mostly a segment of spur gear with a thin rim. In these studies, the gear segment was typically constrained using certain boundary conditions at the cut ends and a point load along the line of action was applied to a single tooth in order to simulate the forces imposed on a sun or an internal gear by the mating planet. This segment of the gear was modelled by using the conventional finite element (FE) method with the same boundary conditions applied in order to simulate the actual support conditions. These models do not

*Corresponding author. Tel.: +1-419-530-8224; fax: +1-419-530-8206.
E-mail address: akahrama@eng.utoledo.edu (A. Kahraman).

0022-460X/03/$ - see front matter
doi:10.1016/S0022-460X(03)00122-6

include the other gears in the planetary gear set as the forces acting on the planet–sun gear and planet–internal gear meshes are represented by a single point force applied mostly on a single tooth along the line of action. While these models were instrumental in qualitatively describing the influence of the rim thickness on the bending stresses of an internal gear, they were not fully capable of describing the behavior observed in a number of experiments on this subject matter [12,15–18]. The accuracy of the stress predictions were strongly dependent on the suitability of the conventional FEM meshes to simulate the tooth, the boundary conditions imposed to represent the actual support conditions, and the assumption that a point load can fully describe the actual loads on planet mesh. Since large portions of the internal gear and the other gears (planets and the sun gear) are left out of these models, it was not possible to investigate the effect of internal gear rim thickness on the overall behavior of the planetary gear set including its influence on the stresses of planets and the sun gear and the load sharing amongst the planets. Similarly, an accurate prediction of the shape and the amount of gear deflections was also not possible for the same reasons.

Two recent studies by the first author [2,6] employed a non-linear deformable-body model of an entire planetary gear set to investigate the impact of rim flexibilities, especially of the internal gear, on gear stresses and planet load sharing under static conditions. These studies indicate that reducing rim thickness of the gears improve functionality of the gear set by minimizing the adverse effects of gear and carrier manufacturing errors and by improving the planet load-sharing characteristics under quasi-static conditions. However, these benefits come at the expense of increased gear stresses. The practical design question of how thin gear rim thicknesses can be without any durability problems is not possible to answer based on these static analyses alone. It is expected that behavior of the planetary gear set changes under dynamic conditions as the system flexibility is increased, potentially increasing gear stresses to a certain extent.

1.1. Objectives and scope

The main objective of this study is to investigate the dynamic effects on gear stresses as a function of gear rim thickness parameters and the number of planets in the system. A deformable-body dynamic model will be used to simulate a typical automotive automatic transmission planetary unit. The model includes all of the gears of the planetary gear set in their deformable form, addressing the shortcomings of the previous simplified models cited above. A new rim thickness parameter will be introduced that takes into account the size of the gears. The model will be used to quantify the impact of the gear rim flexibilities on dynamic gear stresses. The relationship between the bending modes of the gears and the number of planets in the system will also be demonstrated quantitatively.

2. Deformable-body dynamic model

An analysis of planetary gear sets using conventional FE packages presents a number of major challenges stemming from the geometric, kinematic and loading characteristics of this application. The width of a typical gear contact zone is at least an order of magnitude smaller than the other gear dimensions, requiring a very refined mesh near the contact. As the contact zone travels over

the tooth surfaces, such a fine mesh must follow it resulting in a very refined FE mesh over the entire tooth surfaces. The computational time required by such a fine FE model is often overwhelming [19] even under static conditions. In addition, the level of geometric accuracy required from a gear contact analysis is so high that a conventional finite element approach fails to deliver. Finally, there are major difficulties in generating an optimal mesh that is capable of modelling the stress gradients in the critical regions, especially at the tooth root, while minimizing the total number of degrees of freedom of the entire model.

The contact model employed in this study overcomes such difficulties by using FEM and surface integral methods in conjunction. The details of this previously developed model can be found in a paper by Vijayakar [20]. The model uses finite element method to compute relative deformations away from the contact zone. Use of finite elements also allows an accurate representation of complex shapes that planetary gears have. The nearfield deformations in the contact zone are computed using semianalytical techniques based on the half-space solution for a concentrated load. This eliminates the need for a very refined mesh along the tooth surfaces. The nearfield semianalytical solution and the farfield finite element solutions are matched at a matching surface. The finite element model implemented here uses separate interpolation schemes for the displacements and coordinates. The tooth surfaces are modelled by elements that have a very large number of co-ordinate nodes, and can therefore accurately represent the involute shape and surface modifications. In the fillet region, the elements have a large number of displacement nodes to correctly capture the steep stress gradients [6]. The model uses a hierarchical representation of the system that is built from many substructures, with each substructure in turn being composed of many substructures. This allows reducing the computational and memory requirements significantly.

In a planetary gear set, each gear goes through large rotations according to kinematic relationships. The elastic deformations of the gears are much smaller and must be superposed on the rigid-body motions. By choosing a gear co-ordinate frame that follows the rigid-body motion, the finite element displacement vector $\mathbf{x}_{if}$ for gear i can be represented by a linear system of differential equations [21],

$$\mathbf{M}_{ffi}\ddot{\mathbf{x}}_{fi} + \mathbf{C}_{fi}\dot{\mathbf{x}}_{ffi} + \mathbf{K}_{ffi}\mathbf{x}_{fi} = \mathbf{f}_{fi}, \tag{1}$$

where $\mathbf{f}_{fi}$ is the vector of external loads. Rayleigh's damping model is used here in the form

$$\mathbf{C}_{ffi} = \mu\mathbf{M}_{ffi} + \eta\mathbf{K}_{ffi}, \tag{2}$$

where μ and η are constant coefficients. Representing the rigid-body motions of the reference frame by $\mathbf{x}_{ir}$ and combining it with Eq. (1) results in

$$\begin{bmatrix} \mathbf{M}_{ffi} & \mathbf{M}_{fri} \\ \mathbf{M}_{rfi} & \mathbf{M}_{rri} \end{bmatrix} \begin{Bmatrix} \ddot{\mathbf{x}}_{fi} \\ \ddot{\mathbf{x}}_{ri} \end{Bmatrix} + \begin{bmatrix} \mathbf{C}_{ffi} & \mathbf{C}_{fri} \\ \mathbf{C}_{rfi} & \mathbf{C}_{rri} \end{bmatrix} \begin{Bmatrix} \dot{\mathbf{x}}_{fi} \\ \dot{\mathbf{x}}_{ri} \end{Bmatrix} + \begin{bmatrix} \mathbf{K}_{ffi} & \mathbf{K}_{fri} \\ \mathbf{K}_{rfi} & \mathbf{K}_{rri} \end{bmatrix} \begin{Bmatrix} \mathbf{x}_{fi} \\ \mathbf{x}_{ri} \end{Bmatrix} = \begin{Bmatrix} \mathbf{f}_{fi} \\ \mathbf{f}_{ri} \end{Bmatrix}. \tag{3}$$

The equations for each gear are assembled into the entire planetary gear system to obtain the overall matrix equation of motion

$$\mathbf{M}\ddot{\mathbf{x}} + \mathbf{C}\dot{\mathbf{x}} + \mathbf{K}\mathbf{x} = \mathbf{F}. \tag{4}$$

For the solution of the above equation, a time-discretization scheme based on the Newmark method is used as described in detail by Parker et al. [21].

2.1. Example system

An example planetary system is chosen here to represent an automotive gear set in the configuration of a final drive unit of a front-wheel-drive automatic transmission. Here, the internal gear is held stationary and the other two central members are given the duties of input and output. Gear rim deflections can be especially important in a final drive planetary gear set since it is the most heavily loaded gear set in the transmission. Also, the internal gear-case interface forms a direct vibration/force path to the case for noise generation. The same configuration applies to other applications such as automotive all-wheel-drive transfer case reduction units and rotorcraft reduction units as well. The design parameters of the example system are listed in Table 1. The FE models of the same system are shown in Fig. 1. Here, the carrier, the sun gear and the internal gear are input, output and the reaction members, respectively. Two variations of the system with three ($n = 3$) and four ($n = 4$) equally spaced planets are considered. Nominal tooth profile modifications are applied on each gear as stated in Table 1. The internal gear is held stationary within the housing by means of 15 equally spaced, straight external splines. Sufficient radial clearance is allowed at both the minor and major radii of the spline interface for allowing the internal gear to deflect, reflecting the real-life application. The planets, the carrier and the sun gear are supported in radial direction by isotropic bearings.

2.2. Rim thickness parameter

One conventional way of quantifying a gear rim thickness has been comparing it to the height of the teeth. This so-called back-up ratio is given mathematically for external (sun or planet) and internal (ring) gears as

$$\Lambda_{ext} = \frac{R_{root} - R_{bore}}{R_{OD} - R_{root}}, \quad \Lambda_{int} = \frac{R_{OD} - R_{root}}{R_{root} - R_{minor}}, \tag{5}$$

where R_{OD}, R_{root}, R_{bore} and R_{minor} are the outer, root, inner (bore) and minor radii, respectively, as defined in Fig. 2. The back-up ratio Λ has been widely used especially by gear designers since it is

Table 1
Design parameters of the example system (All dimensions are in mm unless specified)

	Sun	Pinion	Internal
Number of teeth	34	18	70
Module	1.5	1.5	1.5
Pressure angle, deg	21.3	21.3	21.3
Circular tooth thickness	1.895	2.585	1.895
Hob tip radius	0.2	0.2	—
Fillet radius	—	—	0.5
Outer radius, R_{OD}	26.37	15.25	58.275–64.825
Root radius, R_{root}	23.00	11.875	55.00
Minor radius, R_{minor}	—	—	51.725
Bore radius, R_{bore}	13.15–20.473	7.488–9.85	—
Linear tip modification	0.010	0.010	—
Starting roll angle of relief, deg	21	27	—

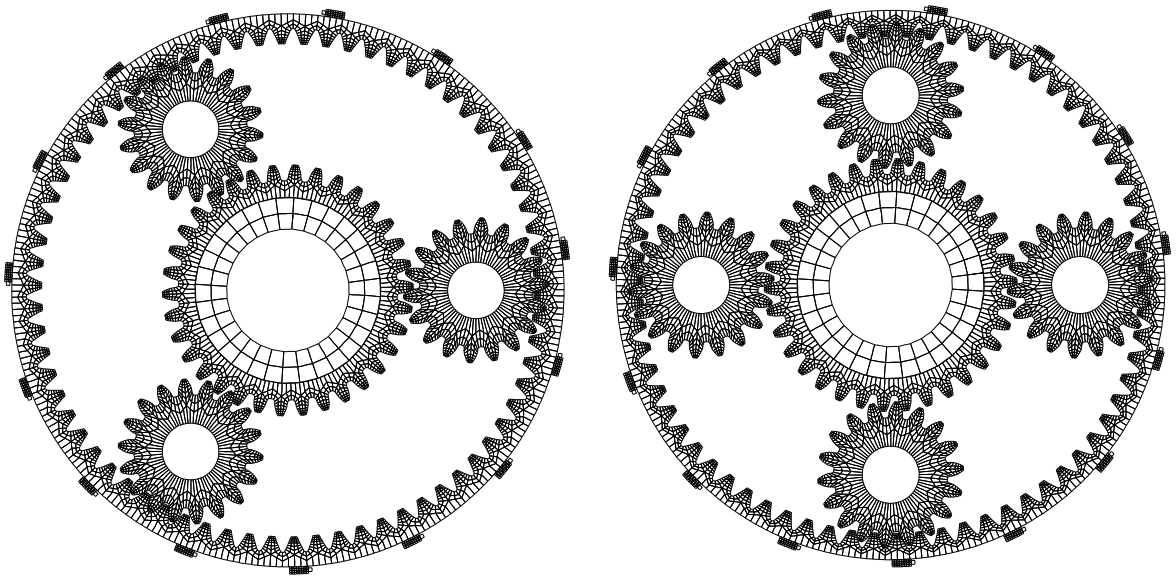

(a) (b)

Fig. 1. Deformable-body dynamic models of the example system: (a) $n = 3$ and (b) $n = 4$.

easy to calculate. However, it has a major shortcoming, as the size of the gear is not factored in. Two gears having the same rim thickness and tooth height would have the same values of Λ even if their radii were different. Obviously, the gear with larger radius has more flexibility and hence should exhibit larger deflections. In a planetary gear set, assuming the tooth heights and rim thickness values for the internal gear sun gear and planets are all equal, one obtains $\Lambda_s = \Lambda_p = \Lambda_r$, where subscripts s, p and r denote sun, planet and internal (ring) gears, respectively. Yet a sun or planet gear of the same Λ value should be significantly stiffer than an internal gear.

This deficiency of the conventional back-up ratio Λ with regard to relating to the dynamic behavior accurately can be avoided by introducing a new rim thickness parameter Γ defined as the ratio of the rim thickness to the root radius. This new rim thickness parameter takes into account the size of the gear. For external and internal gears shown in Fig. 2,

$$\Gamma_{ext} = \frac{R_{root} - R_{bore}}{R_{root}}, \quad \Gamma_{int} = \frac{R_{OD} - R_{root}}{R_{root}}. \tag{6}$$

3. Results and discussion

In contrast to the static analysis, the dynamic analysis at a given input speed and input torque value takes significantly more computational effort. Damping and mass matrices must also be constructed and included in the calculations in accordance with Eq. (4) in addition to the stiffness matrix and the force vector. Since the steady-state response is of particular interest, the simulation must be carried out for a reasonably long period of time to surpass the transient region. In

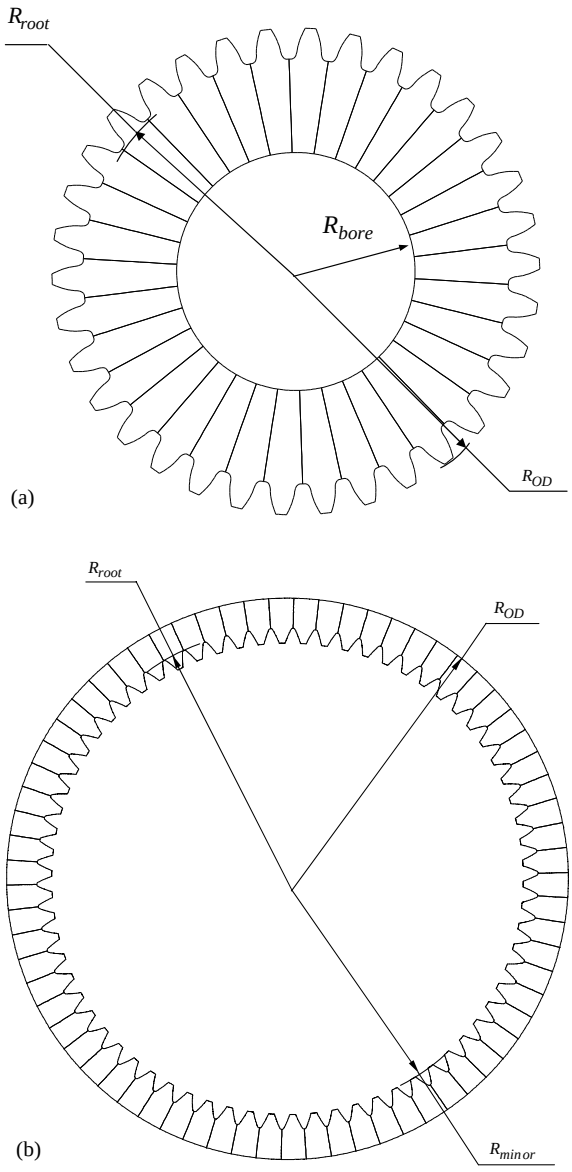

Fig. 2. Dimensions required for the definition of the rim thickness parameters for (a) an external gear and (b) an internal gear.

addition, the time increment must be small enough in order to capture all dynamic motions to a desired resolution.

In order to reach the region of steady state motions, each analysis was performed in four distinct ranges. In the first range, a single-point static analysis was performed to define initial conditions for the dynamic analysis. The second range is the ramp-up stage from zero to the desired speed in a relatively short time period with a small number of time steps (about 50) followed by a 1800-time-step analysis at the desired speed to rotate the carrier by a complete

rotation. In this range, the analysis time increment was kept relatively course since the purpose here is to pass through the transients as quickly as possible. Finally, the fourth range is formed by a refined 8200 time-step analysis (about one-third carrier rotation) from which the steady state response is obtained. The analysis in the last range is extended further if the repeatability of the stress time histories are not acceptable meaning the transient motions are still present. Damping coefficients of $\mu = 7.1(10)^{-4}$ and $\eta = 1.4(10)^{-7}$ s were used in this example case. These damping values were such that the system reaches its steady state after one to two complete carrier rotations.

3.1. *Influence of rim thickness on dynamic gear stresses*

All four ranges combined, one single analysis at a given speed and torque value took nearly 19 h of computational time on a high-end personal computer. Therefore, it was not feasible to perform extensive parametric studies of rim thickness under dynamic conditions. Instead, a rather limited objective is adapted here: *What are the dynamic consequences of using a flexible gear* (*say internal gear*) *compared to a rigid one over a large operating speed range?*

Initially, two cases were chosen for the comparison. The first case represents a flexible internal gear with $\Gamma_r = 0.06$ ($\Lambda_r = 1.0$) and the second case considers the same planetary gear set, now with a rigidly supported internal gear (no rim deflections). As all gears for both cases are identical except the boundary conditions, system mass and stiffness matrices remain the same resulting in the same Rayleigh damping values. Here, the system has three equally spaced planets and the internal gear is splined in the rigid housing using 15 equally spaced straight splines as shown in Fig. 1(a). In this example case, the other gears have relatively thicker rims compared to the

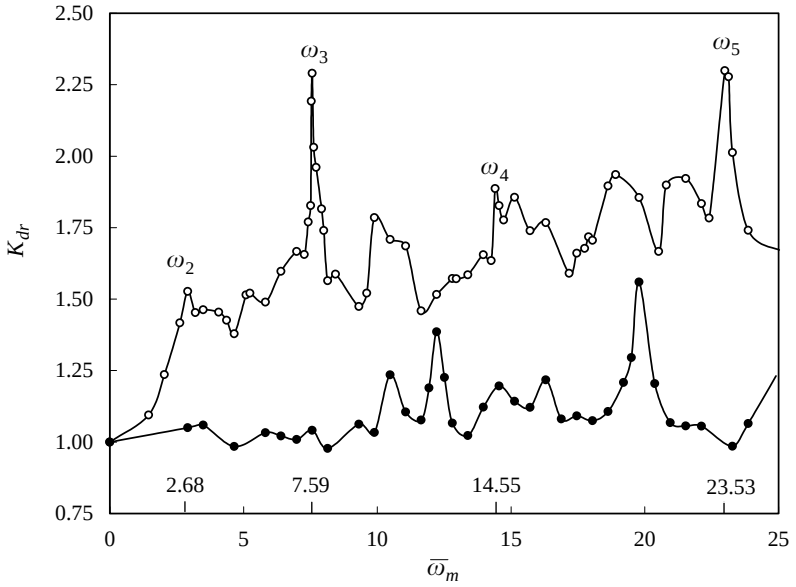

Fig. 3. Internal gear dynamic stress factors as a function of the normalized gear mesh frequency: ◦, $\Gamma = 0.06$; •, rigid.

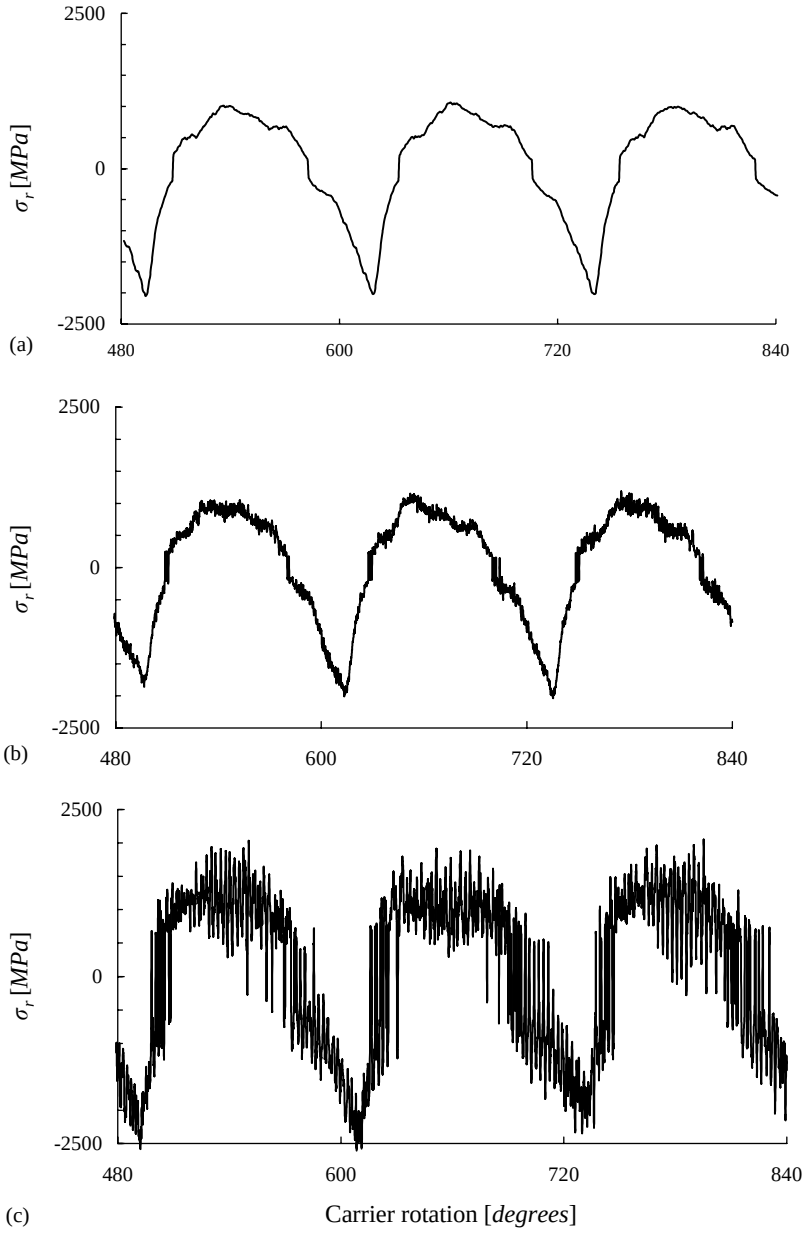

Fig. 4. Maximum internal gear bending stress history for a system having $\Gamma_r = 0.06$ ($\Lambda_r = 1.0$) at (a) $\bar{\omega}_m = 0$ (quasi-static), (b) $\bar{\omega}_m = 4.65$, and (c) $\bar{\omega}_m = 7.59$.

internal gear with $\Gamma_s = 0.44$ and $\Gamma_p = 0.5$. The input (carrier) torque was 1500 N m. Both sun gear and the planet carrier were piloted by radial bearings.

The carrier speed Ω_c was varied within a range between 0 and 4000 r.p.m., corresponding to a gear mesh frequency range of $\omega_m = 0$–$33\,000$ rad/s (5250 Hz) where $\omega_m = 2\pi\Omega_c Z_r/60$ and Z_r is the number of teeth of the internal gear. At each ω_m value, the four-range transient analysis

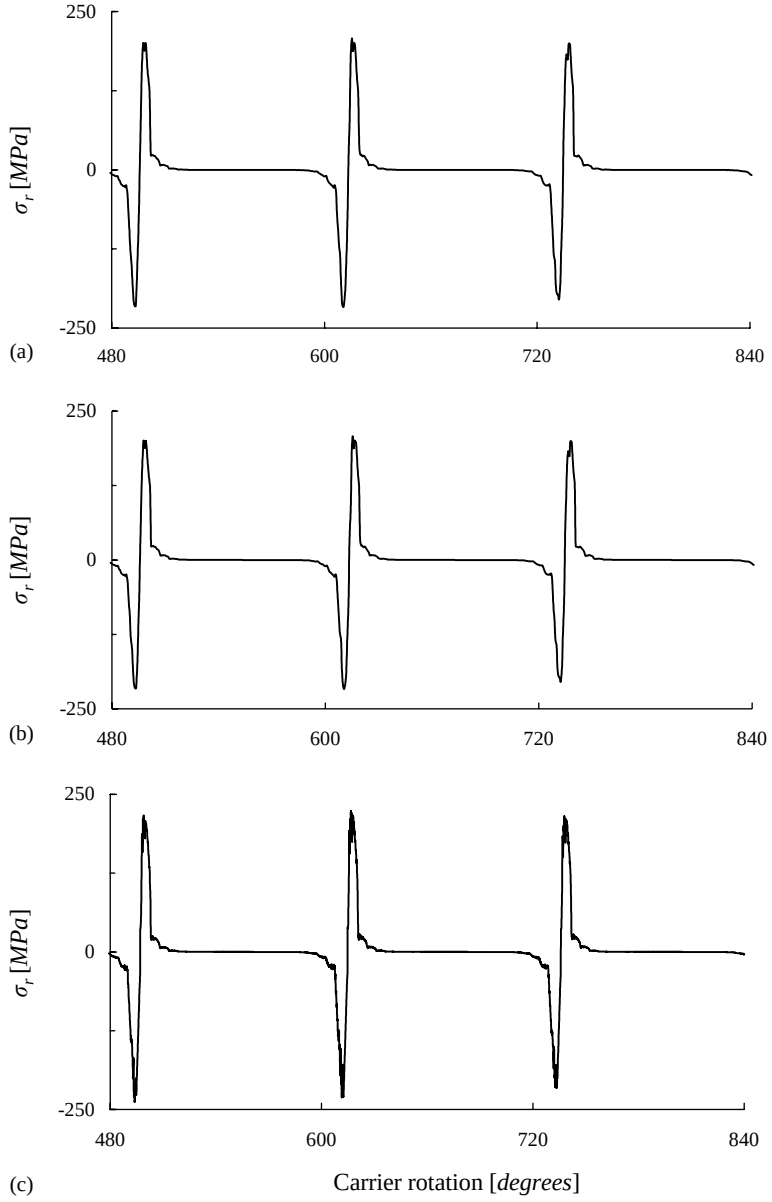

Fig. 5. Maximum internal gear bending stress history for a system having a rigid rim at (a) $\bar{\omega}_m = 0$ (quasi-static), (b) $\bar{\omega}_m = 4.65$, and (c) $\bar{\omega}_m = 7.59$.

outlined above was performed and the maximum values of the steady state gear stresses are recorded. Dynamic stress factors K_d for each gear at that speed were calculated as the ratio of the maximum dynamic stress $\sigma_{di,max}$ to the corresponding maximum quasi-static stress $\sigma_{si,max}$. For a gear i:

$$K_{di} = \frac{\sigma_{di,max}}{\sigma_{si,max}}, \quad i = s, p, r. \tag{7}$$

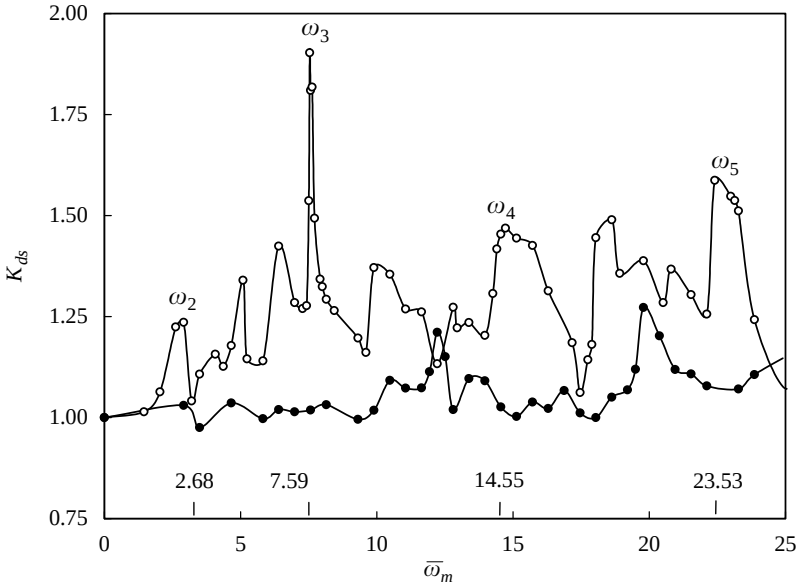

Fig. 6. Sun gear dynamic stress factors as a function of the normalized gear mesh frequency. ◦, $\Gamma = 0.06$; •, rigid.

The bending natural frequencies of a thin ring structure are given by [22]

$$\omega_q = \frac{q(q^2-1)}{\sqrt{1+q^2}}\sqrt{\frac{EI}{\mu R^4}}, \quad q = 2, 3, 4, \ldots, \tag{8}$$

where q is the modal index, E is the modulus of elasticity, I is the area moment of inertia of the cross-section, μ is the mass per unit length, and R is the radius of the ring. A resonance peaks associated with the internal gear bending modes might exist when the gear mesh frequency is equal to a bending natural frequency, i.e., $\omega_m \approx \omega_q$. Accordingly, if one normalizes the gear mesh frequency by using Eq. (8) such that $\bar{\omega}_m = \omega_m/\sqrt{EI/(\mu R^4)}$, bending mode resonance peaks should appear at $\bar{\omega}_m = q(q^2-1)/\sqrt{1+q^2} = 2.68, 7.59, 14.55, 23.53, \ldots$.

Fig. 3 compares maximum internal gear dynamic factors K_{dr} for two cases, namely a system having a flexible internal gear with $\Gamma_r = 0.06$ ($\Lambda_r = 1.0$) and a system having an internal gear with a rigid rim. Here, an internal gear tooth at the midpoint between two splines was considered. The first observation is that as $\bar{\omega}_m$ is increased, K_{dr} is increased for both cases showing the contribution of dynamic conditions to stress levels. The increase in K_{dr} is significantly larger for the system with the flexible internal gear reaching up to $K_{dr} = 2.3$ (the maximum dynamic stress experienced by the internal gear is 2.3 times larger than the maximum stress levels under quasi-static conditions) within the range of $\bar{\omega}_m$ considered. The steady state, internal gear stress time histories at selected $\bar{\omega}_m$ values for $\Gamma_r = 0.06$ ($\Lambda_r = 1.0$) are displayed in Fig. 4. Here, the impact of dynamic motions on internal gear stresses is rather obvious. On the other hand, the example stress time histories given in Fig. 5 for the rigid internal gear show signs of limited dynamic effects, in line with Fig. 3.

Apparent resonance conditions are evident in Fig. 3 at mesh frequencies $\bar{\omega}_m = 2.68, 7.59, 14.55$ and 23.53 ($\Omega_c = 460, 1300, 2600$ and 3900) r.p.m. for $\Gamma_r = 0.06$ ($\Lambda_r = 1.0$) corresponding to the internal gear bending modes ω_2–ω_5. Since the K_{dr} amplitudes are much lower and no resonance

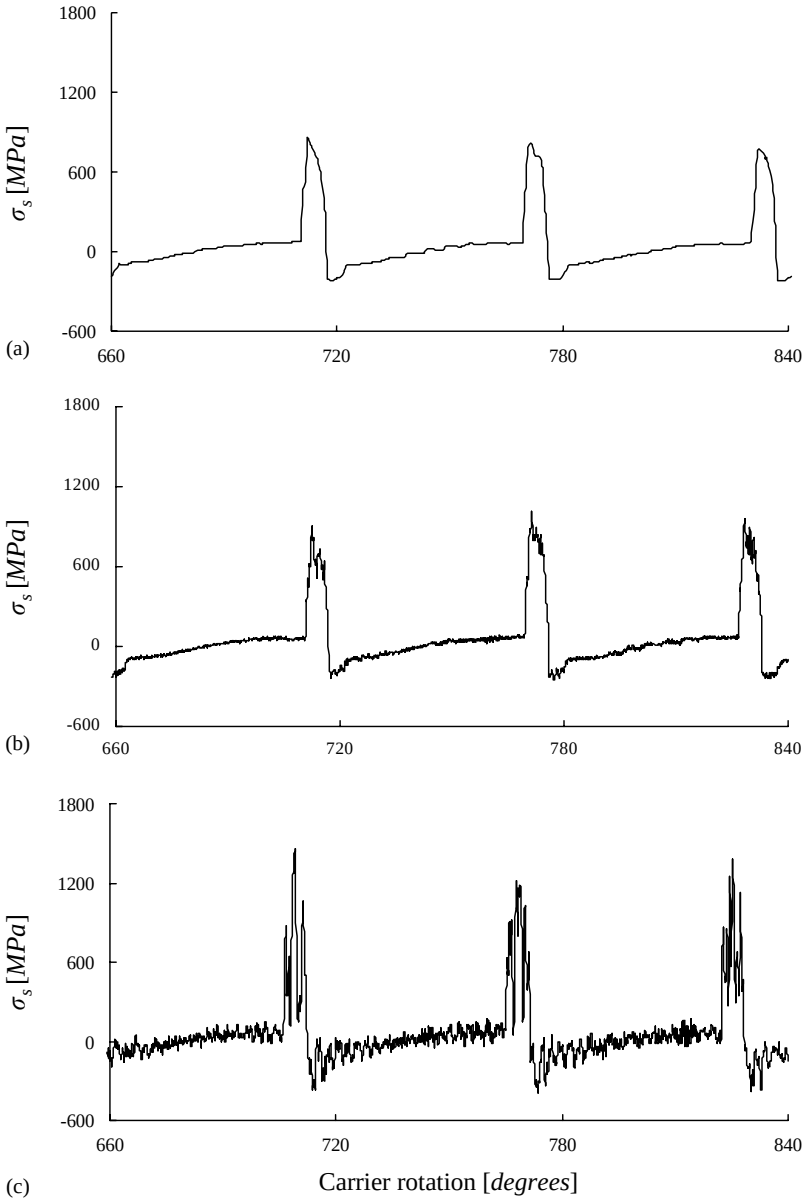

Fig. 7. Maximum sun gear bending stress history for a system having $\Gamma_r = 0.06$ ($\Lambda_r = 1.0$) at (a) $\bar{\omega}_m = 0$ (quasi-static), (b) $\bar{\omega}_m = 4.65$, and (c) $\bar{\omega}_m = 7.59$.

condition exists for the rigid internal gear at the same frequency values, these resonance peaks can be attributed to internal gear bending natural modes. It is also clear from Fig. 3 that the resonance peak corresponding to ω_3 is the most severe one.

A very similar behavior is observed for the sun gear dynamic factors as well for the same cases of $\Gamma_r = 0.06$ and rigid internal gear rim. As shown in Fig. 6, for $\Gamma_r = 0.06$ ($\Lambda_r = 1.0$), K_{ds} values climb steadily with increasing $\bar{\omega}_m$ and experience rather large-amplitude resonance peaks at $\bar{\omega}_m =$

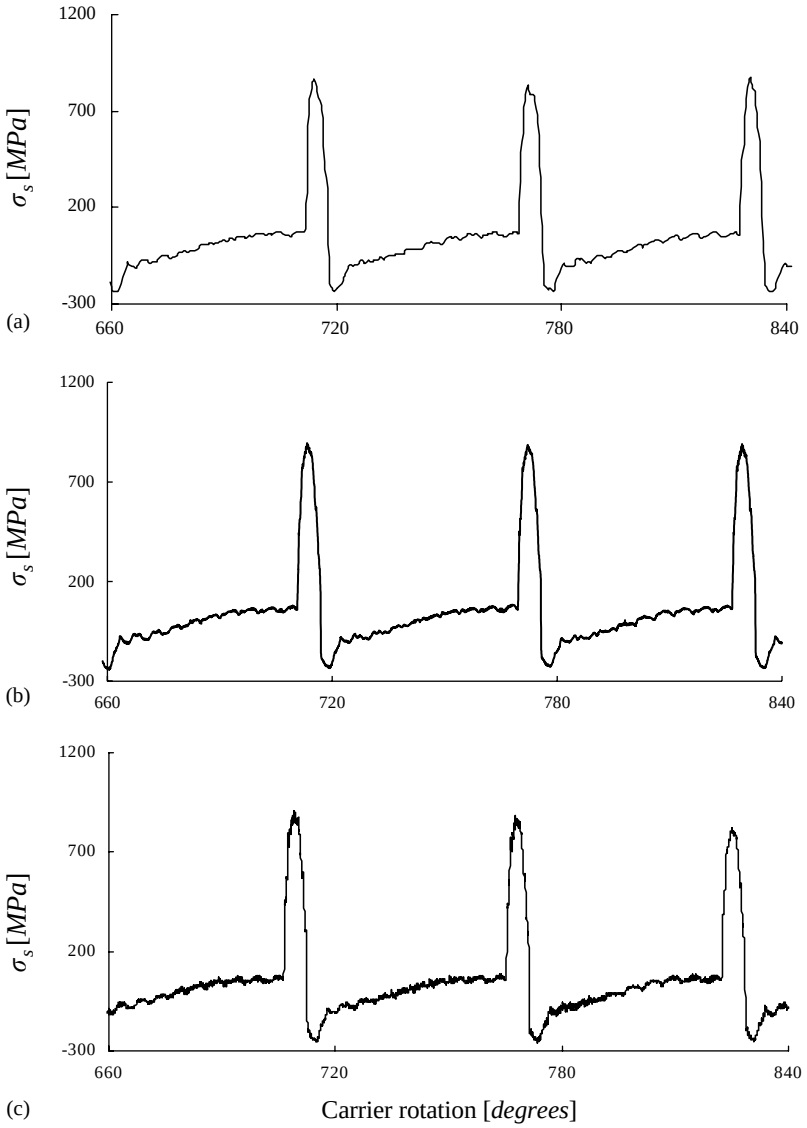

Fig. 8. Maximum sun gear bending stress history for a system having a rigid rim at (a) $\bar{\omega}_m = 0$ (quasi-static), (b) $\bar{\omega}_m = 4.65$, and (c) $\bar{\omega}_m = 7.59$.

2.68, 7.59, 14.55 and 23.53, again corresponding to the internal gear bending frequencies at ω_2 to ω_5. Sun gear steady state stress time histories at several $\bar{\omega}_m$ values for $\Gamma_r = 0.06$ are displayed in Fig. 7. Here, the impact of dynamic motions on sun gear stresses is again evident. Meanwhile, sun gear stress time histories given in Fig. 8 for the case rigid internal gear of Fig. 6 again exhibit limited dynamic effects.

The impact of the internal gear flexibility on planet dynamic stress factor is also very significant as illustrated in Fig. 9 for the same two cases as above. Again, K_{dp} values increase steadily with $\bar{\omega}_m$ and pass through large-amplitude resonance peaks at the same internal gear bending frequencies

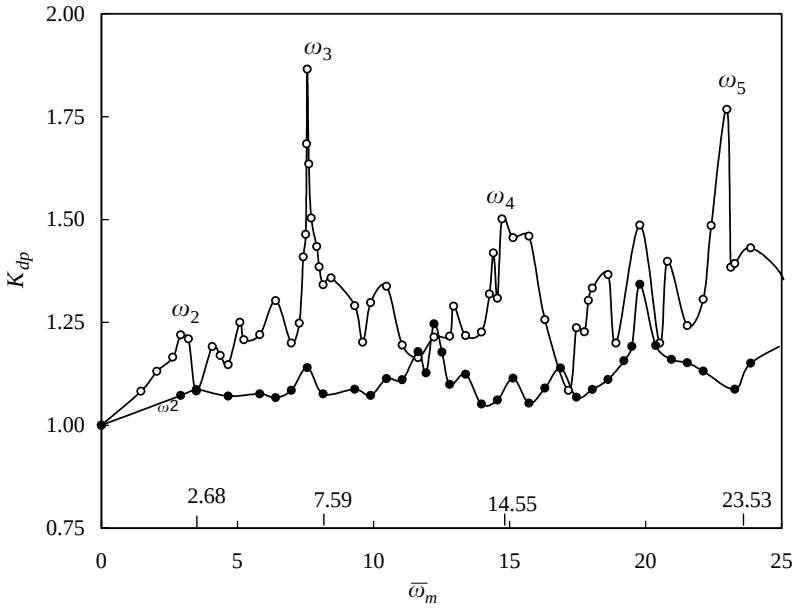

Fig. 9. Planet gear dynamic stress factors as a function of the normalized gear mesh frequency. ◦, $\Gamma = 0.06$; •, rigid.

as before. Steady state stress time histories of the planet gear at several $\bar{\omega}_m$ values displayed in Fig. 10 for $\Gamma_r = 0.06$ ($\Lambda_r = 1.0$) again emphasize the dynamic effects on planet gear stresses while the stress time histories given in Fig. 11 for the system with a rigid internal gear again show rather limited dynamic effects.

Two other resonance peaks are apparent in Figs. 3, 6 and 9 that are not associated with the internal gear bending modes. For the case of rigid internal gear, these two resonance peaks are at nearly $\bar{\omega}_m = 12.3$ and 19.9 ($\Omega_c = 2100$ and 3400 r.p.m.) and their frequencies are both reduced somewhat if the internal gear is flexible. These resonance peaks were found to correspond to the transverse-torsional natural modes of the planetary gear set as described in detail in previous discrete-parameter dynamic modelling studies [23]. The observed change in these resonance frequencies suggests that the predictions of discrete parameter models that assuming rigid gear rims should involve a certain amount of error. It would be safe to conclude that a deformable body analysis is necessary especially when the gear rims are rather flexible, not only for including the rim bending modes but also for the more accurate prediction the planetary gear set modes.

3.2. *Relationship between the bending modes and the number of planets*

In Figs. 3, 6 and 9, although resonance peaks associated with the all bending natural modes of $q = 2$–5 were observed to exist for the system with three planets ($n = 3$), the resonance peak at $\bar{\omega}_m = 7.59$ corresponding to $q = 3$ was the most significant one, bringing the issue of a possible link between the number of planets and the excitability of a particular bending mode. Under quasi-static conditions, the internal gear deflects to a mean triangular shape (when the deformations are exaggerated) that has characteristically the same shape as the $q = 3$ mode.

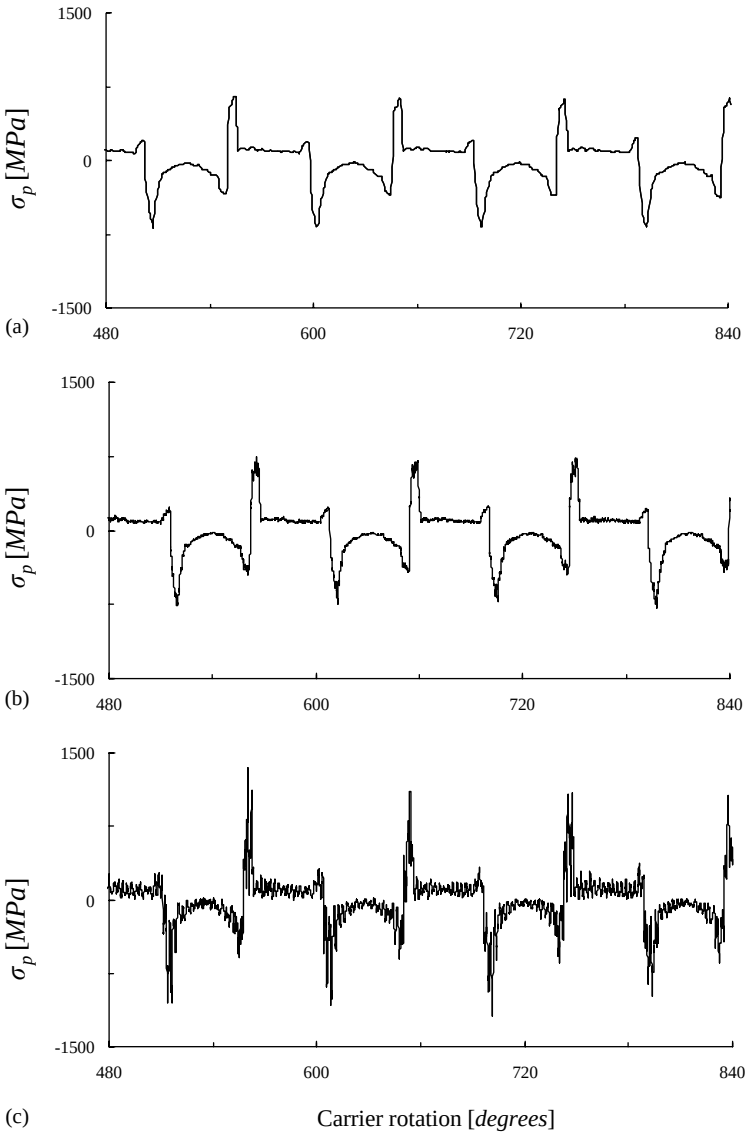

Fig. 10. Maximum planet gear bending stress history for a system having $\Gamma_r = 0.06$ ($\Lambda_r = 1.0$) at (a) $\bar{\omega}_m = 0$ (quasi-static), (b) $\bar{\omega}_m = 4.65$, and (c) $\bar{\omega}_m = 7.59$.

In order to investigate this issue further, a four-planet version of the same system shown in Fig. 1(b) having $\Gamma_r = 0.06$ ($\Lambda_r = 1.0$) is analyzed in the vicinity of resonance peaks of $q = 3$ and 4 at $\bar{\omega}_m = 7.59$ and 14.55, respectively. Fig. 12 compares maximum K_{ds} values of two gear sets with $n = 3$ and 4, both having $\Gamma_r = 0.06$. In the vicinity of $\bar{\omega}_m = 7.59$, the resonance amplitude is much more severe when $n = q = 3$ reaching a maximum value of 1.9 while this value is only 1.4 for the four-planet system. Meanwhile, in the vicinity of $\bar{\omega}_m = 14.55$, the resonance peak amplitudes are much higher when $n = q = 4$. The system with $n = 4$ results in a maximum K_{ds} value of 1.9 while

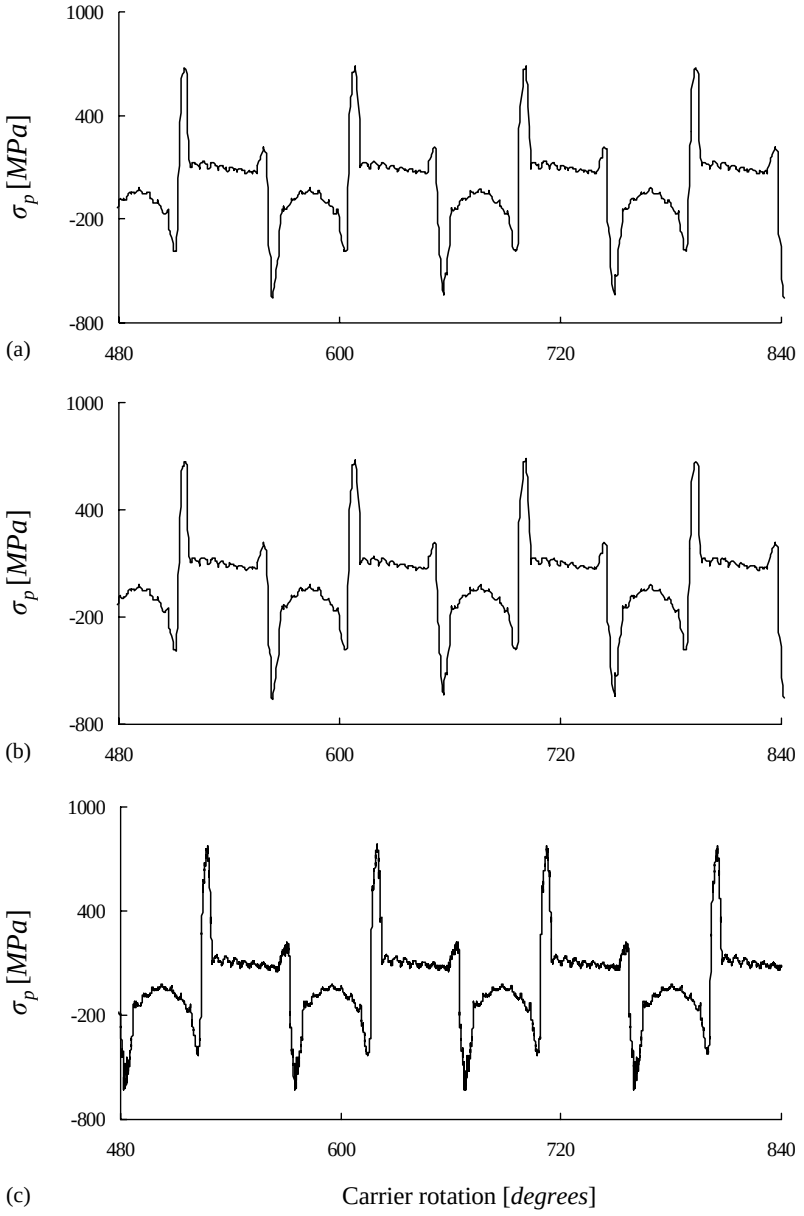

Fig. 11. Maximum planet gear bending stress history for a system having a rigid rim at (a) $\bar{\omega}_m = 0$ (quasi-static), (b) $\bar{\omega}_m = 4.65$, and (c) $\bar{\omega}_m = 7.59$.

the system having $n = 3$ yields only $K_{ds} = 1.45$. This suggests that any qth gear bending mode is excited most severely when $n = q$. This itself can be a sufficient reason in practical gear design to increase the number of planets in case there is a bending resonance within the operating speed range of the gear set.

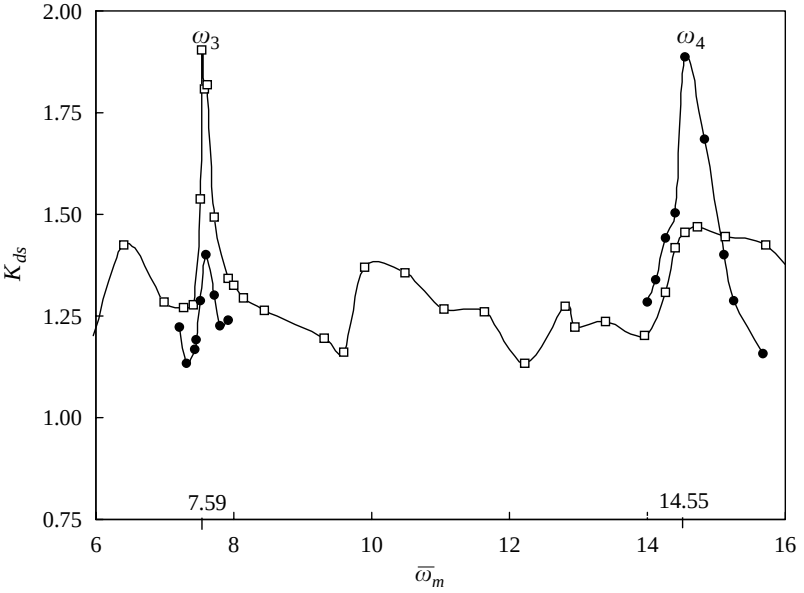

Fig. 12. Influence of n on K_{sd} given $\Gamma_r = 0.06$ ($\Lambda_r = 1.0$): □, $n = 3$; ●, $n = 4$.

4. Conclusions

In this study, the effect of flexibility of gears on the dynamic behavior of a planetary gear set is investigated. An existing contact mechanics formulation is employed to model a typical automotive automatic transmission final drive planetary unit. The model considers each gear as a deformable body and meshes them to predict loads, stresses and deformations. A new generalized gear rim thickness parameter that includes the gear radius is proposed in place of the conventional back-up ratio. The influence of internal gear rim flexibility on dynamic stresses and gear rim deflections is quantified. Based on the results presented, dynamic gear tooth bending stress values were found to be significantly higher for all of the gears for a flexible internal gear as compared to the rigid internal gear, reaching their maximum values at the bending natural frequencies of the internal gear. It was also shown that the internal gear bending resonance peaks are the most significant if the number of planets in the system match the modal index of the bending mode. This study also indicates that a deformable body analysis is necessary especially when the gear rims are rather flexible for both including the rim bending modes properly and predicting the overall planetary gear set modes more accurately.

Acknowledgements

We thank Dr. S. Vijayakar of Advanced Numerical Solutions, Inc. for his guidance and for making the gear analysis package 2DPLANETARY available.

References

[1] J.R. Colbourne, The geometric design of internal gear pairs, AGMA Technical Paper, 87 FTM 2, 1987.
[2] A. Bodas, A. Kahraman, Influence of manufacturing errors and design parameters on the static planet load sharing behavior of planetary gear sets, International Motion and Power Transmission Conference, Fukuoka, Japan, 2001.
[3] F. Cunliff, J.D. Smith, D.B. Welbourne, Dynamic tooth loads in epicyclic gears, Transactions of the American Society of Mechanical Engineers, Journal of Engineering for Industry (1974) 578–584.
[4] T. Hidaka, Y. Terauchi, K. Nagamura, Dynamic behavior of planetary gear (7th report, influence of the thickness of the ring gear), Bulletin of JSME 22 (1979) 1142–1149.
[5] B. Balasubramanian, Dynamische Lastferteilung in Planetensatzen, Ph.D. Dissertation, University of Karlsruhe, Germany, 1993.
[6] A. Kahraman, S. Vijayakar, Effect of internal gear flexibility on the quasi-static behavior of a planetary gear set, American Society of Mechanical Engineers Transactions, Journal of Mechanical Design 123 (2001) 408–415.
[7] S.H. Chang, R.L. Huston, J.J. Coy, A finite element stress analysis of spur gears including fillet radii and rim thickness effects, Transactions of the American Society of Mechanical Engineers, Journal of Mechanical Design, 82-WA/DE-35, 1982, pp. 1–4.
[8] G.D. Bibel, S.K. Reddy, M. Savage, R.F. Handschuh, Effect of rim thickness on spur gear bending stress, NASA Technical Memorandum 104388, 1991.
[9] P. Clerici, A. Girotti, A. Perazzolo, Comparison of web stress concentration factors and safety margins for a thin webbed spur gear subjected to static and cyclic loading conditions, American Society of Mechanical Engineers International Power Transmission and Gearing Conference, DE-Vol.43-1, pp. 53–58, 1992.
[10] C.A. Brazakis, D.R. Houser, Finite element and experimental analysis of the effects of thin-rimmed gear geometry on spur gear fillet stresses, International Gearing Conference, Newcastle upon Tyne, UK, pp. 41–46, 1994.
[11] T. Hidaka, Y. Terauchi, M. Nohara, J. Oshita, Dynamic behavior of planetary gear (3rd report, displacement of ring gear in the direction of line of action), Bulletin of JSME 20 (1977) 1663–1672.
[12] T.H. Chong, A. Kubo, Simple stress formulae for a thin-rimmed spur gear. Part 3: examination of the calculation method and stress state of internal spur gear pair, Transactions of the American Society of Mechanical Engineers, Journal of Mechanisms, Transmissions, and Automation in Design 107 (1985) 418–423.
[13] S. Oda, K. Miyachika, Root stress of thin-rimmed internal spur gear supported with pins, JSME International Journal 30 (1987) 646–652.
[14] J.P. Vaujany, H.C. Kim, M. Guingand, D. Play, Effects of rim and web on stresses of internal cylindrical gears, Proceedings of the ASME International Power Transmission and Gearing Conference DE-88 (1996) 73–80.
[15] H. Linke, C. Jahn, Bending load on internal gears of planetary gear sets, AGMA Technical Paper, 97FTM7, 1997.
[16] A. Kahraman, Static load sharing characteristic of transmission planetary gear sets: model and experiment, SAE Paper, 1999-01-1050, 1999.
[17] T.L. Krantz, Gear tooth stress measurements of two helicopter planetary stages, NASA Technical Memorandum 105651, 1992.
[18] M. Botman, Vibration measurements on planetary gears of aircraft turbine engines, Journal of Aircraft 17 (1980) 351–357.
[19] M. Valco, Planetary Gear Train Ring Gear and Support Structure Investigation, Ph.D. Dissertation, Cleveland State University, 1992.
[20] S. Vijayakar, A combined surface integral and finite element solution for a three-dimensional contact problem, International Journal for Numerical Methods in Engineering 31 (1991) 525–545.
[21] R. Parker, S. Vijayakar, T. Imajo, Nonlinear dynamic response of a spur gear pair: modeling and experimental comparisons, Journal of Sound and Vibration 237 (2000) 435–455.
[22] J.P. Den Hartog, Mechanical Vibrations, Dover, New York, 1985.
[23] A. Kahraman, Planetary gear train dynamics, American Society of Mechanical Engineers Transactions, Journal of Mechanical Design 116 (1994) 713–720.